WAVEGUIDES

A. L. Eldredge, Editor, and V. G. Price

This chapter describes the rectangular waveguide system which transfers microwave power from the klystrons to the disk-loaded accelerator. In addition to the transfer of microwave power, this system provides for monitoring the power level of the klystron outputs. The phase of a beam-induced wave in the disk-loaded waveguide is also monitored once in each 40 ft of accelerator length.

A key boundary condition for the design of the waveguide network is based upon the decision to feed four 10-ft sections of the disk-loaded waveguide from one klystron. Consequently, the waveguide network must either have a high-power phase shifter in each 10-ft accelerator feed or be made with sufficient accuracy and temperature stability to make independent phase adjustment of the separate waveguide feeds unnecessary. Consideration of cost and operational factors led to the latter design solution. During operation, phase adjustments are made only at the RF inputs to the klystrons.

High emphasis was placed on reliability. A major reliability question concerned the RF windows in the waveguide system between the klystrons and the accelerator. A window is needed at each klystron to provide a vacuum seal which is transparent to RF in the output waveguide. This allows each klystron to be independently evacuated, processed, and tested, and then stored until it is needed for service on the accelerator. Early in the design program there was doubt regarding the feasibility of designing a window capable of handling the high-peak and average powers needed for the accelerator without providing gaseous cooling on the output side of the window. However, the use of gaseous cooling within the waveguide system demanded that a second window be provided in series to prevent the gas from entering the accelerator. Moreover, it would have been necessary to pressurize the gas to enable it to withstand the high-voltage gradients in the waveguide without breakdown.

A puncture or crack in any of the 245 secondary windows in the waveguide system would then result in the accelerator becoming filled with gas, which would immediately make it inoperable. Consideration of this serious consequence led to the decision to use only a single in-line window (attached to the klystron) and to evacuate the waveguide region between the klystron and the accelerator. This decision, of course, complicated the window design problems but, in spite of formidable difficulties, a window meeting these requirements was designed, as discussed in Chapter 10. A further consequence of the decision to use a single in-line window was the necessity of developing a waveguide valve. This valve would allow reflectionless transmission of RF power when in the open position but would be an effective vacuum seal when it was closed, thus allowing klystron replacement without disturbing the accelerator vacuum. Such a valve was successfully developed and is described later in this chapter.

For reasons outlined above, the rectangular waveguide system was designed to operate in high vacuum ($\approx 10^{-8}$ torr). The decision to evacuate the waveguide system also necessitated the development of reliable vacuum directional couplers, loads, power dividers, and vacuum pumpout orifices with high conductance and negligible RF coupling. Special fabrication techniques also had to be developed to provide the nominal 48,000 ft of rectangular waveguide.

A fundamental requirement for the overall machine design was that it should allow the initial energy specification to be doubled without requiring significant structural changes in the klystron gallery and accelerator housing, and without increasing the length of the disk-loaded waveguide. To be compatible with this design philosophy, the rectangular waveguide network was designed to have sufficient flexibility to accommodate any subsequent addition to the number of klystron stations with minimum accelerator downtime, while keeping the cost of the initial network as low as possible. The flexibility was achieved by careful planning of the waveguide layout and by the use of additional flange joints that allow the network to be disassembled and reconnected to accommodate an increased number of klystron stations.

General specifications established to meet the waveguide system requirements are given in Table 11-1.

11-1 Waveguide layout

The specific configuration for the waveguide network was determined by the conformations of the principal elements of the system and by the requirement for flexibility to add, conveniently, additional klystron stations with little accelerator downtime. The primary elements affecting the layout included microwave loads, RF couplers, power dividers, vacuum pumpouts, waveguide valves, and the mechanisms allowing rapid replacement of the klystrons.

The short-slot hybrid junction was used for the power dividers in preference to a simple shunt or series T-junction because it is much less sensitive

Table 11-1 General specifications of waveguide system

Operating frequency	2856 MHz $\pm$ 3 MHz
Input reflection coefficient	$\lvert S_{11}\rvert < 0.07$
Power transmission capacity	24 MW peak, 21 kW average
Phase deviations of output signals relative to an input reference phase	$\pm 3°$ ($+360° n$, where n may be as high as 23)
Vacuum operating level	10^{-7} torr at full RF power, 10^{-8} torr at zero RF power
Gas burst rate	Less than 1 burst/hour average at full RF power after processing
Temperature tolerances	$\pm 2°$F

to load impedance variation. More specifically, a T-junction subjected to impedances that produce VSWR's of 1.10 in each of the two outputs will have a power division difference that can, in the worst case, be 0.8 dB. For the same load condition the power output imbalance from the short-slot hybrid is 0.1 dB in the worst case.

Folded hybrids and short-slot, sidewall hybrids were much easier to adapt to the waveguide network than either the top-wall hybrids or magic T's. Furthermore, sidewall hybrids were found to have higher-peak power handling capacity[1] than magic T's, folded hybrids, or simple T-junctions. The short-slot hybrid of the Riblet[2] design proved to be the most suitable because of its relatively simple configuration and good electrical characteristics.

The basic module of the waveguide network consists of the waveguide components necessary to connect two klystrons to 80 ft of accelerator structure. Figure 5-17 illustrates this basic rectangular waveguide network module. The rectangular waveguide system for the injector, designed by Tsang and Keicher,[3] is shown in Fig. 11-1. This network provides for switching from the on-line klystron to a standby klystron within seconds and provides power to the prebuncher and buncher as well as to the injector disk-loaded waveguide section. The prebuncher and buncher feeds have independent phase and power adjustments. The special waveguide network for the positron sources is illustrated in Fig. 11-2.

A fundamental problem concerned the relative motion of the klystron gallery and accelerator housing due to normal earth shifting and settling. In addition to accommodating this relative motion, the waveguide network had to function properly in the presence of temperature excursions encountered during installation and start-up, shut-down cycles associated with machine operations. To accommodate these conditions, the waveguide layout was designed so that the only fixed tie points were at the klystrons. The fixed point was achieved by reinforcing the directional coupler with stainless steel plates and bolting it to the klystron frame. The klystron frame consists of two vertical cylindrical steel pipes 20 ft apart, bridged by a steel I-beam. The I-beam has a yoke which supports the klystron, together with its permanent magnet and

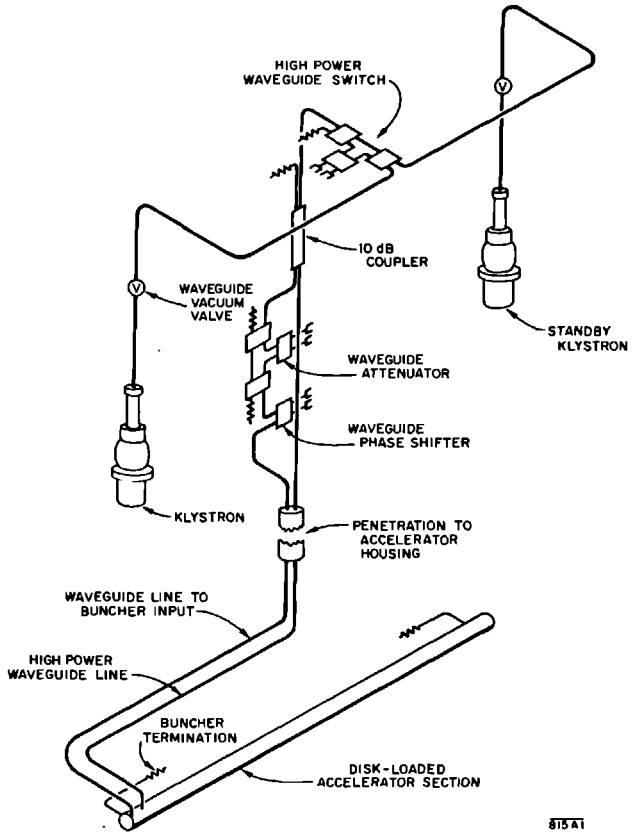

Figure 11-1 Waveguide network in the injector area.

pulse transformer tank. The yoke design provides an indexing system which insures that the klystron vertical output waveguide matches the flange of the rectangular waveguide network. The reinforced directional coupler also provides the connection point of the vacuum system to the waveguide network in the klystron gallery.

The rectangular waveguide crossbar assembly is supported as shown schematically in Fig. 11-3. The flexible supports at points A and B are achieved by spring couplings to the klystron frame. The vertical loads due to the weight of the waveguides in the vertical penetrations are transferred to the klystron frame by the same springs. The klystron frame is adjustable both vertically and horizontally by means of a jack pad between the floor and the bottom of the steel vertical pipes. Hence any changes in the relative positions of the klystron gallery and accelerator housing can be compensated for by adjusting the klystron frame. This arrangement and procedure prevent the waveguide network from producing loads on the 40-ft girders, which could cause serious misalignment of the accelerator structure. Figure 11-4 is a photograph of the klystron, the support frame, and the crossbar assembly.

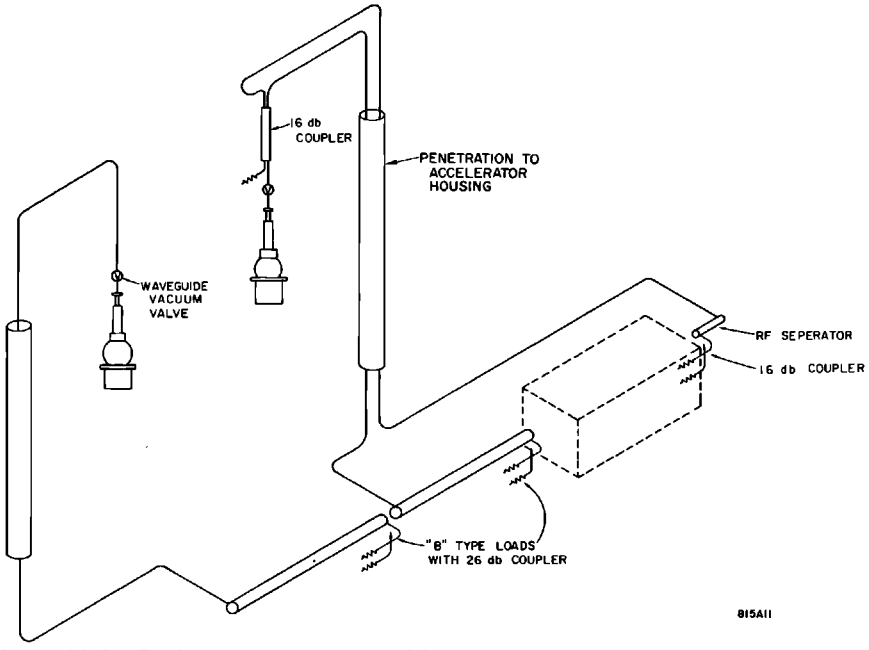

Figure 11-2 Positron source waveguide arrangement.

The waveguide layout was designed to be as nearly symmetrical as possible, in spite of the restrictions imposed by the need for alternating the direction of the input feeds to the 10-ft accelerator sections and by the decision to have flexibility to accommodate additional klystron stations. The primary asymmetry is caused by the latter requirement which necessitated locating the klystron

Figure 11-3 Schematic of waveguide attachment to klystron support frame.

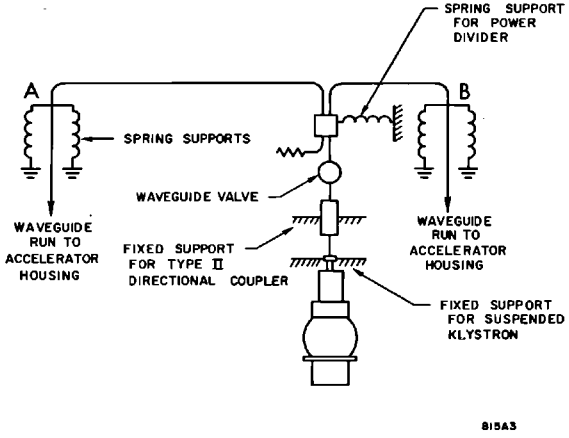

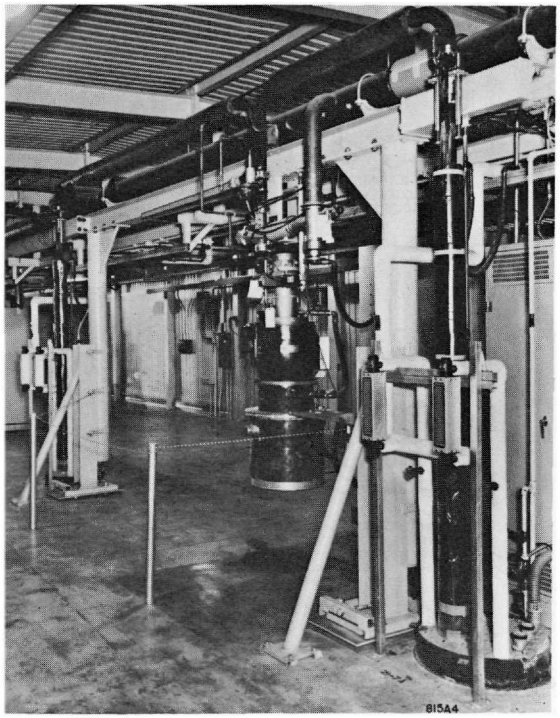

Figure 11-4 Klystron support frame with waveguide and klystron attached.

so that one waveguide run from the klystron is about twenty guide-wavelengths longer than the other run from the same klystron. The resultant asymmetry required careful attention to the design of the waveguide network, including the methods of cooling, phase adjustment, and mechanical support.

11-2 Waveguide selection

Cross section

The internal dimensions for the rectangular waveguide cross section were set at 1.340 × 2.840 in., with a tolerance of ± 0.005 in. Factors leading to this cross-section included both microwave and vacuum considerations.

Initial technical design considerations suggested the possibility of using the rectangular waveguides both as the microwave transmission system and as the evacuation lines between the klystron gallery and the accelerator housing for the accelerator structure. In addition to possible reduction and simplification in vacuum components, the larger cross section that would be

necessitated by vacuum conductance requirements would give some microwave advantages such as lower dispersion and attenuation. However, economic consideration established that it was far less expensive to use the smallest waveguide cross section that could reliably meet the microwave requirements and use separate periodic stainless steel manifolds to evacuate the accelerator structure. These factors led to the design of the vacuum system as described in Chapter 23.

The factors involved in determining the waveguide cross section, in addition to those already discussed, included material selection, cooling methods, phase stability, and fabrication methods to process approximately 48,000 ft of waveguide. Consideration of the vacuum requirements, electrical performance, and fabrication problems led to the selection of high-purity low-oxygen content (not more than 10 parts per million) copper as the waveguide material. The only other suitable materials were silver and aluminum. The use of silver would yield a waveguide with 2% less attenuation than one made from copper; however, its extreme cost outweighs such a small improvement in attenuation. An aluminum waveguide has an attenuation 15% greater than copper, which is an intolerable increase, and particularly so in view of the relatively small difference in the cost of the two materials for a fabricated, installed, rectangular waveguide network.

The waveguide network design makes it essential to have excellent phase stability because there are no high-power phase shifters (with the exception of the one in the injector). This requirement places critical dimensional stability tolerances on the waveguide cross section. Pressures and forces that can produce mechanical deflections are due to evacuation of the waveguide, the loads imposed by the waveguide weight, and changes in distance between the klystron gallery and the accelerator housing. The change in distance between the klystron gallery and the accelerator housing due to normal earth motion is a very slowly varying function; hence periodic mechanical adjustment of the klystron support frame can maintain this force at a very small value. The principal source of waveguide dimensional change is the elastic deformation of the copper caused by atmospheric pressure when the waveguide is evacuated.

Elastic deformation can be minimized by making the waveguide walls sufficiently thick. However, there is a reasonable balance between allowable deformation and the cost of the waveguide. The cross section of an unperturbed rectangular waveguide of inside width a and height b is shown in Fig. 11-5. Virgile[4] studied deformation of waveguide subject to internal pressure. Experimental data showed that evacuated waveguide deforms as illustrated in Fig. 11-6. Virgile's data gives $\Delta a_0/\Delta b_0$ as 0.21 for pressurized WR-284 waveguide, which has the same internal dimensions as the SLAC waveguide. Assuming sine wave deformation, the phase shift per unit length caused by such perturbations of the waveguide walls may be shown to be[5]

$$\frac{\Delta\phi}{L} = \frac{2\lambda_g}{a^2}\left[\frac{\Delta a_0}{a} + \frac{1}{3}\frac{\Delta b_0}{b}\right] \tag{11-1}$$

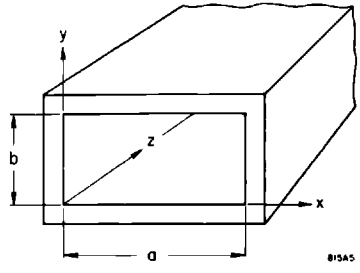

Figure 11-5
Waveguide dimensions.

where λ_g is the guide wavelength and the other symbols have meanings as illustrated in Figs. 11-5 and 11-6. Substituting $\lambda_g = 6.023$ in., $a = 2.840$ in., $b = 1.340$ in., and $\Delta a_0/\Delta b_0 = 0.21$ in Eq. (11-1) yields the result $\Delta\phi/L = 0.17°/\text{ft}/0.001$ in. change in the dimension b at the center of the broad face of the waveguide.

Experimental, evacuated, waveguide cavities, 4 ft long, were fabricated to provide empirical data on the variation in phase shift as a function of wall thickness and atmospheric pressure. The results of measurement and computation of phase shift per unit length are plotted on Fig. 11-7 using values of Δb_0 which were determined by Skarpaas.[6] The shift in resonant frequency, corrected for the dielectric constant of the air-water vapor in the cavity, was measured when the cavity was evacuated. The measured, incremental phase shift for the 0.157-in. sample waveguide approached the value that was accepted as the maximum allowable; hence this wall thickness was specified as the minimum. The nominal wall thickness was specified as 0.173 in. with tolerances on the internal dimensions of ± 0.005 in. and tolerances on the external dimensions of ± 0.010 in.

Barometric pressure at SLAC seldom falls outside the limits of 29.0 to 30.5 in. of mercury. By interpolation of the upper experimental curve of Fig. 11-7, a phase shift of 0.023°/ft/in. of mercury change in barometric pressure can be predicted for a waveguide with 0.173-in. wall thickness. A 12-ft length of waveguide was fitted with vacuum windows on its ends and inserted in a chamber in which the external pressure could be varied while maintaining an internal vacuum. The incremental phase shift per unit length measured by a

Figure 11-6 Waveguide deformation when evacuated.

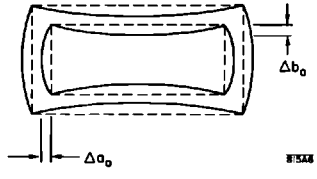

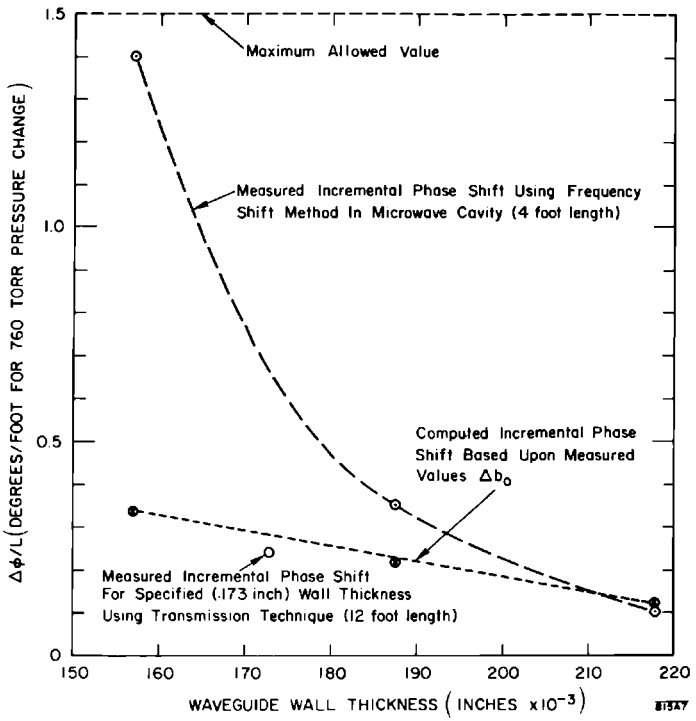

Figure 11-7 Measured and computed values of incremental phase shift for evacuated waveguide with wall thicknesses of 0.157, 0.187, and 0.218 in.

transmission method was found to be approximately 0.008°/ft/in. change in barometric pressure. Work hardening of the annealed copper, from repeated cycling, produced some difficulty in repeating the measurements but reflected what would actually be encountered in operation. It was concluded that the expected differential phase shifts due to changes in atmospheric pressure in the SLAC area with the asymmetric waveguide should be no greater than 0.2°.

The long-term plastic creep of the copper in the rectangular waveguide under operating conditions is estimated to be sufficiently small that it will be 8 to 10 yr before any trim tuning of the waveguide will be required.

The cooling necessary for temperature and, hence, for length stability is provided by water flowing through a 1 × 1½-in. rectangular tube brazed on one broad wall of the waveguide, as shown in Fig. 11-8. Phase shift measurements versus water pressure in the cooling water tube were made, using the cavity frequency shift method, on two 6-ft samples. The frequency shift in the evacuated 6-ft waveguide cavity was measured as the coolant channel was pressurized to 80 psi. A large initial inelastic deformation was observed, but after reaching the elastic deformation region, the furnace-brazed samples

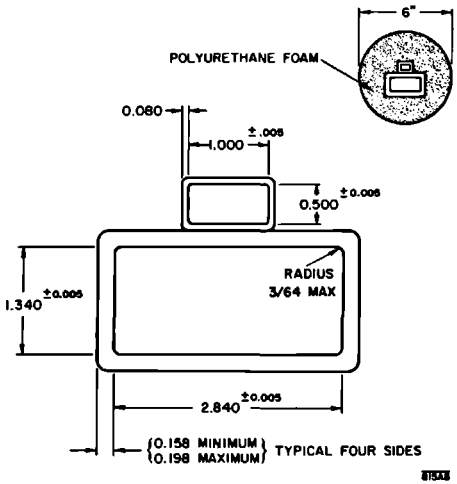

Figure 11-8 Specified waveguide and cooling tube dimensions. Cooling tube is shown in its brazed position on the rectangular waveguide.

showed an incremental phase shift of 8.3×10^{-4} deg/ft/psi of variation in water pressure. It was concluded from this that no significant phase error would be incurred due to coolant pressure fluctuations or to turning the water off and on.

Key factors in the successful fabrication of the rectangular waveguide network and the disk-loaded waveguide were the quality of copper used and the choice of fabrication techniques. The copper requirements for these two components of the accelerator were more than 2 million lb in ingot form. To assure quality, steps in the copper processing were controlled from the refinery state through fabrication of the mill shapes, including the special cross sections for the rectangular waveguide and cooling tube.

The entire 48,000 ft of waveguide was processed at SLAC. All operations culminating in the final installation of the waveguide network were performed using the same quality-control standards and techniques as used in high-power vacuum tube manufacture. These techniques include high-quality chemical cleaning and high-temperature hydrogen brazing procedures. The rectangular water cooling tube was brazed to the rectangular waveguide in a 17-ft deep hydrogen furnace. A substantial saving in the cost of the waveguide was achieved by specifying that random lengths would be acceptable. Long lengths were made by butt brazing shorter pieces of the rectangular waveguide together after the cooling tube brazing was completed. Precise joints were made possible by sizing the male and female ends of the rectangular waveguides to a tolerance of ± 0.001 in. and then brazing them together as shown in Fig. 11-9.

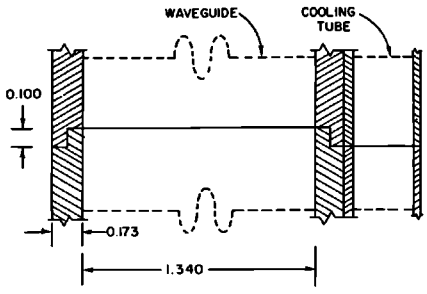

Figure 11-9 Waveguide butt-joint configuration.

Several random lengths of waveguide (with brazed cooling tubes) were arranged in a closed horizontal array and brazed together to form the required long lengths, such as the 38-ft pieces needed to extend through the penetrations between the klystron gallery and the accelerator housing. Before brazing the array of short pieces, they were filled with hydrogen through a capoff flange, and the hydrogen was burned at the output capoff flange. The series of brazes necessary to complete the assembly were then sequentially made with an oxygen–hydrogen ring flame burner. The silver–copper eutectic used in the braze was hand fed when the joint reached the proper temperature; no preplaced alloy was employed in the butt joints. This method produced excellent joints as verified by metallographic cross sections from samples and by the overall operating success of the machine to date. (At this writing, some of the joints are already 4 yr old).

11-3 Waveguide insulation and heat control

Accuracy of phase relationships and phase stability make it essential that the rectangular waveguide be closely temperature controlled during accelerator operation. The electrical length of a waveguide of length L is given by

$$\phi = \beta_g L \tag{11-2}$$

where β_g is the waveguide phase constant. Differentiating Eq. (11-2) with respect to temperature, T, gives

$$\frac{d\phi}{dT} = \beta_g \frac{dL}{dT} + L\frac{d\beta_g}{dT} \tag{11-3}$$

In the TE_{10} mode, β_g can be expressed as

$$\beta_g^2 = \beta_0^2 - \left(\frac{\pi}{a}\right)^2 \tag{11-4}$$

where $\beta_0 = 2\pi/\lambda_0$ is the free-space phase constant and a is defined in Fig. 11-5.

Therefore,

$$\frac{d\phi}{dT} = \beta_g \frac{dL}{dT} + \frac{L\pi^2}{\beta_g a^3} \frac{da}{dT} \tag{11-5}$$

From the coefficient of linear thermal expansion of the metal, α, one obtains

$$\alpha = \frac{da}{a\,dT} = \frac{dL}{L\,dT} \tag{11-6}$$

Combining Eqs. (11-5) and (11-6) gives

$$\frac{d\phi}{dT} = \frac{\alpha L}{\beta_g} \left[\left(\frac{\pi}{a} \right)^2 + \beta_g^2 \right] \tag{11-7}$$

Combining Eqs. (11-4) and (11-7) gives

$$\frac{d\phi}{dT} = \frac{\alpha L \beta_0^2}{\beta_g} = \frac{2\pi\alpha L \lambda_g}{\lambda_0^2} \tag{11-8}$$

where λ_g is the guide wavelength and λ_0 is the free-space wavelength. The value of α at the operating temperature of 113°F is 9.26×10^{-6}/°F, hence Eq. (11-8) gives $(d\phi/dT) = 0.0141$ electrical degree/ft/°F at the SLAC operating frequency.

Equation (11-8) was experimentally verified over a temperature range of 30°F, with very good agreement between theory and experiment.

Heat is generated in the high-power waveguide by the RF currents flowing in the waveguide walls. The rectangular waveguide itself has a resistive attenuation of about 6.3×10^{-3} dB/ft. In addition, each stainless steel flange pair has an attenuation of about 6.8×10^{-3} dB while the other components of the system have a total attenuation below 0.1 dB. The calculated average loss through a network from a klystron to an accelerator section is 0.54 ± 0.10 dB. Measurements using sliding shorts on the four outputs of a full-scale model gave a network attenuation of 0.5 dB. This attenuation will cause a heat dissipation of approximately 2.4 kW in the rectangular waveguide fed from a klystron delivering 21 kW average power. This power dissipation was verified using a full scale model of the waveguide layout. It is, therefore, necessary that the cooling system should provide close temperature control while dissipating 2.4 kW per accelerator feed and should be capable of handling higher powers when additional klystron stations are added.

The design work done by Lisin[7] led to a cross section for the temperature-stabilized cooling waveguide as illustrated in Fig. 11-8. Water flow rates are 10 gal/min in the full power waveguide and 5 gal/min in the waveguide carrying half-power or less. The 2°F temperature stability requirements made it necessary to use a polyurethane foam insulating jacket as shown in Fig. 11-8 to reduce the cost of temperature control. Insulation was applied to the cross-bar and penetration waveguides. It was unnecessary to insulate the waveguide in the accelerator housing because there is good temperature stability in this area due to the temperature control of the disk-loaded waveguide.

Table 11-2 Calculated power levels at accelerator input ports relative to klystron output

Waveguide network configuration	*Imbalance*	*Branch 1 (dB)*	*Branch 2 (dB)*	*Branch 3 (dB)*	*Branch 4 (dB)*
ABAB	Minimum	−6.52	−6.53	−6.57	−6.58
	Maximum	−6.42	−6.53	−6.57	−6.68
BABA	Minimum	−6.53	−6.51	−6.58	−6.56
	Maximum	−6.53	−6.41	−6.68	−6.56

Asymmetrical division of power from a klystron would result in unequal power dissipation in the accelerator sections and waveguide feeds. This would give rise to temperature and phase shift differentials. Consequently, considerable care was taken to obtain equal power distribution to the four branches of the waveguide network. Table 11-2 gives the best and worst cases of RF power imbalance obtained in the waveguide network, the worst case being due to imperfect division by the power dividers which have a 0.1 dB tolerance. This table gives the total attenuation (including power division) in each of the four branches from any one klystron to an accelerator section. Inspection of Table 11-2 shows that the maximum imbalance between any two feeds is 7% (0.27 dB).

11-4 Electrical phase length considerations

The schematic diagram (Fig. 11-10) of a 40-ft waveguide module defines N_n, the number of guide wavelengths between the klystron output and the four accelerator input ports. If the four branches of the waveguide network are tuned properly, a signal at 2856 MHz at the input will arrive in phase at each of the four output ports. The design phase length of the network is given in Table 11-3 for the two general configurations (ABAB and BABA, identifying the alternating accelerator input coupler orientation shown in Fig. 5-17).

The half-cycle phase length difference between the N_1 and N_2 branches and between the N_3 and N_4 branches corrects for the half-cycle inversion of the signal in passing through a right-handed E-plane bend as compared to the same wave through a left-handed E-plane bend with the same center-line

Table 11-3 Design phase lengths of branches of the wavelength layout

Waveguide network configuration	*Branch phase length in No. of λ_g's*			
	N_1	N_2	N_3	N_4
ABAB	118	121½	134	137½
BABA	123	116½	139	132½

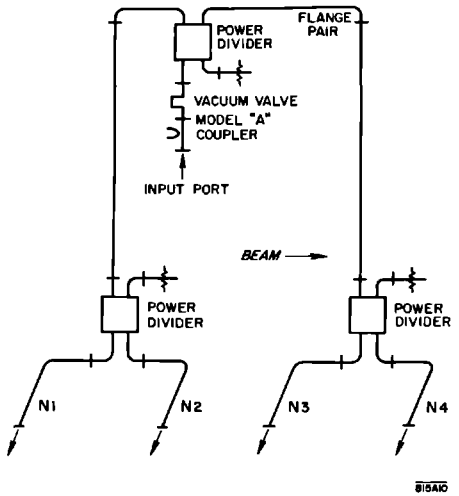

Figure 11-10 Schematic of a 40-ft unit of waveguide network.

length. There is one left-hand E-plane bend in the N_1 and the N_3 branches and one right-hand E-plane bend in the N_2 and N_4 branches. All of the other waveguide bends are H-plane types which do not exhibit this phase reversal.

The manufacturing tolerances of ± 0.005 in. on the internal dimensions of the waveguide correspond to an equivalent phase shift tolerance of $\pm 1.42°$/ft. Prior to phase adjustment of the waveguide layout, the above phase shift tolerance permits the phase shift through one branch of the network to differ as much as 170° from that through another branch. During installation of the waveguide layouts, the pretuning tests showed the phase differences between branches to be typically less than 60° although several with differences close to 180° were encountered.

The phase lengths at 2856 MHz of some waveguide components, such as bends, power dividers, and valves, relative to a reference straight length of waveguide, are given in Fig. 11-11.

Phase length adjustment of the waveguide branches for each klystron was accomplished by Weaver and Alvarez[8] by using a modulated reflection method similar to one suggested by Schafer[9] and later further developed and used by Swarup and Yang[10] to adjust a radio astronomy antenna array.

Each klystron is individually phased by an automatic system to obtain the correct phase relationship between the bunched beam and the wave in one particular accelerator section driven by that klystron. However, the high-power waveguide network must be permanently adjusted so that when the wave is phased correctly with respect to the beam in that one accelerator section, it is also phased correctly in the other three sections driven by that same klystron. Since the accelerator RF input ports are spaced by an integral number of wavelengths (29), the waveguide network branches must be

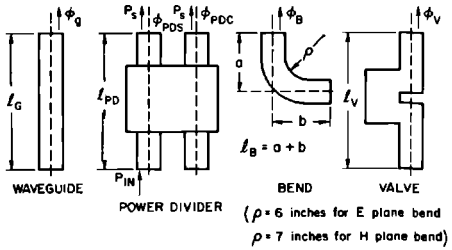

$\Delta\ell_g$	$\Delta\ell_{PDS}$	$\Delta\ell_{PDC}$	$\Delta\ell_B$ "E"	$\Delta\ell_B$ "H"	$\Delta\ell_v$
±0	+0.500"	+2.006"	−3.380"	−4.240"	+10.385"

Figure 11-11 Phase lengths of some waveguide components relative to straight waveguide at 2856 MHz.

adjusted to be equal in phase length, or to differ by only integral numbers of wavelengths.

The modulated reflection method for phase adjustment uses a separate diode-modulated reflector, or "modulator flange," at each of the four accelerator output ports. A 2856-MHz cw signal was fed to the input port of the waveguide network (see Fig. 11-12), then one reflector at a time was modulated at 1 kHz, and each return signal was compared in a phase bridge with a much larger unmodulated reference signal. The resultant signal will not exhibit a

Figure 11-12 Block diagram of phasing machine.

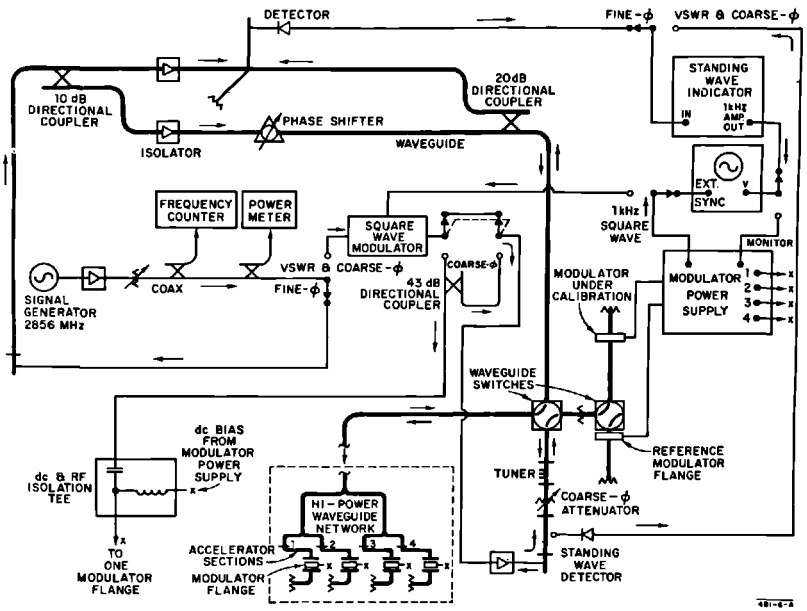

1-kHz amplitude modulation when the reference signal and the carrier of the modulated reflected signal are out of phase by 90°. While measurements are being made on one branch, the diodes in the other three modulator flanges are not switched, but are dc biased to cause little reflection. This allows comparison of the phase lengths of the four branches, subject to the half-cycle ambiguity of the reflection method. The half-cycle ambiguity is then resolved by a standard, transmission phase measurement using the modulator flanges as waveguide-to-coax adapters with a long coaxial cable providing the return path to the input port of the waveguide network. Instability in the coaxial cable limits the accuracy of this method to about 10°.

In the fine-phase (modulated reflection) measurement, the modulator power supply switches one of the four modulator flanges at a 1 kHz rate, forward-biases the other three, and triggers the oscilloscope sweep. The calibrated, dielectric slab phase-shifter is adjusted to produce a null in the 1-kHz amplitude modulation of the sum signal at the detector. The differences in phase shifter settings for the four branches of the network are direct measures of the phase length differences. The standing-wave indicator conveniently doubles as a 1-kHz tuned preamplifier for the detected amplitude modulation of the sum signal. The oscilloscope displays this amplitude modulation and serves also as the synchronous detector which resolves the quarter-cycle ambiguity. The standing-wave detector is used also in a separate measurement to measure the input reflection of the network after tuning. Additional facilities permit calibration of the reflection phases of the modulator flanges and monitoring of drift in the phasing machine.

The modulator flange (Fig. 11-13) consists of a diode switch mounted in a special stainless steel, S-band waveguide flange. Both sides of the flange are machined to form vacuum seals with the waveguide flanges. A point-contact germanium diode is spring loaded against the end of a post across the waveguide. Two adjustable tuning screws in the plane of the diode are used for

Figure 11-13 Modulator flange.

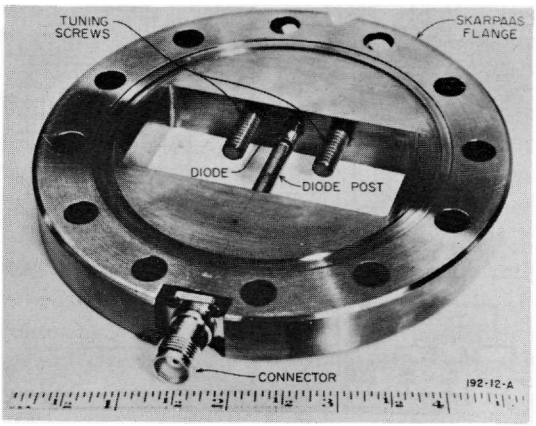

matching. The tuning screws and the diode post, which connects to the center conductor of a TNC fitting on the flange circumference, are vacuum sealed with Teflon O-rings. Thin gold plating on top of copper plating improves the calibration accuracy and the shelf life of the stainless steel flanges. When the flange is properly tuned, reverse biasing of the diode creates a large shunt admittance across the waveguide, which causes almost complete reflection. Forward biasing creates only a small shunt admittance, which causes little reflection. The tuning screws are adjusted so that the phases of the sums of the small and large reflections are the same in all four modulators. Because the diodes exhibit a nonlinear phase-versus-voltage characteristic, square-wave modulation simplifies understanding and analysis of the circuit. The modulator power supply switches the diode bias signal at a 1 kHz rate from -20 V to $+100$ mA. When the diode is reverse biased, the modulator flange serves as a waveguide-to-coax adapter with stable phase characteristics and a transmission loss of about 20 dB. Between the diode support post and the flange body, there is a capacitive reactance of about 1.4 ohms at 2856 MHz, which provides some isolation between the bias circuit and the microwave reflector circuit. Since a modulator flange is primarily a precision reflector, and only incidentally a waveguide-to-coax adapter, the 20-dB transmission loss is preferable to less isolation. Frequent recalibrations locate the position of the equivalent plane of reflection to better than $\pm 0.3°$. The major source of calibration error is the small movement due to slight distortion of the internal parts of the flange modulator during its installation. The modulator flange is the most critical component of the system.

The actual phase adjustments of the network were performed by permanently indenting the waveguide walls with special C-clamps having 12-in. jaws. Smooth indentations over a length of several feet easily produce phase shifts up to 60° between branches, which is generally the maximum correction required. A few networks were out of adjustment by almost 180° and required clamping over longer lengths to prevent significant reflections. Bowing in of the narrow wall of the waveguide decreases its phase length, and bowing in of the broad wall (with consequent bowing-out effects on the narrow wall) increases its phase length.

It was found that measurements could be repeated within $\pm 0.1°$. The modulator flanges have a calibration accuracy of better than $\pm 0.3°$, and the networks have a phase stability of better than $\pm 0.5°$. The accelerator sections are within $\pm 2.5°$ of their design lengths. Thus, the overall accuracy of phase adjustment is better than $\pm 4.5°$, allowing $\pm 1.0°$ for temperature instabilities for the accelerator sections.

11-5 Components of the waveguide system

Stringent specifications were applied to the rectangular waveguide components. Consequently, all components had to be specially developed, including the rectangular waveguide itself as discussed above. Because of the anticipated

addition of more klystron stations in the future, all components had to be capable of handling at least 24-MW peak and 21-kW average power. This meant that all reflection coefficients had to be below −30 dB and all component transmission losses had to be not greater than 0.1 dB for the above peak and average powers. Each component was tested at low and high power before installation to insure that the microwave and mechanical characteristics had been achieved.

During the development period, preproduction models of each component were tested and fully evaluated prior to writing final specifications and initiating production. Because only fully developed and tested designs were produced and because the amount of tuning and other operations required during production to produce satisfactory components was minimized, substantial cost savings resulted. Special facilities were set up to simplify production, tuning operations, and testing.

Flow charts were prepared for each item used in the waveguide layout. The charts showed all the detailed steps needed to fabricate, inspect, test, store, and install the various components. The following paragraphs provide brief descriptions of the principal specially developed components of the waveguide system.

Waveguide vacuum valve (Fig. 11-14)

The vacuum valve[11] is an all-metal structure which is used to isolate the evacuated waveguide layout and the accelerator from exposure to air during replacement of the high-power klystron tube used to drive the accelerator.

The microwave structure consists of a resonant iris in the common broad wall of the two adjacent waveguides. The positions of the shorting plates were determined empirically and are the same in all valves. The positions were adjusted so that, in conjunction with the E-plane 90° miter joints, a bilateral standing-wave ratio of 1.08 or less was obtained at the operating frequency prior to tuning. All production units were tuned by squeezing the walls of the input and output waveguide so that the VSWR was reduced to 1.02 or less.

Continuity of wall currents in the upper waveguide section is achieved through the copper gasket and copper-plated mating surfaces in the backseat region.

The vacuum structure of the waveguide valve is composed of the brazed body and plunger subassemblies. The vacuum seal between these subassemblies is made by means of a crush seal joint and a copper gasket. The recurrent vacuum seal for klystron replacement is made by forcing the plunger assembly's circular stepped knife edge into an indium-filled groove concentric with the circular resonant iris in the common broad wall between the two waveguides. The closing force is provided by a lead screw actuator which attaches directly to the plunger assembly. By using concentric machined steps, several sealing edges are achieved simultaneously. More than 200 closures have been obtained on a single seal (i.e., with leak rates $< 24 \times 10^{-8}$ std cm^3 He/sec) in

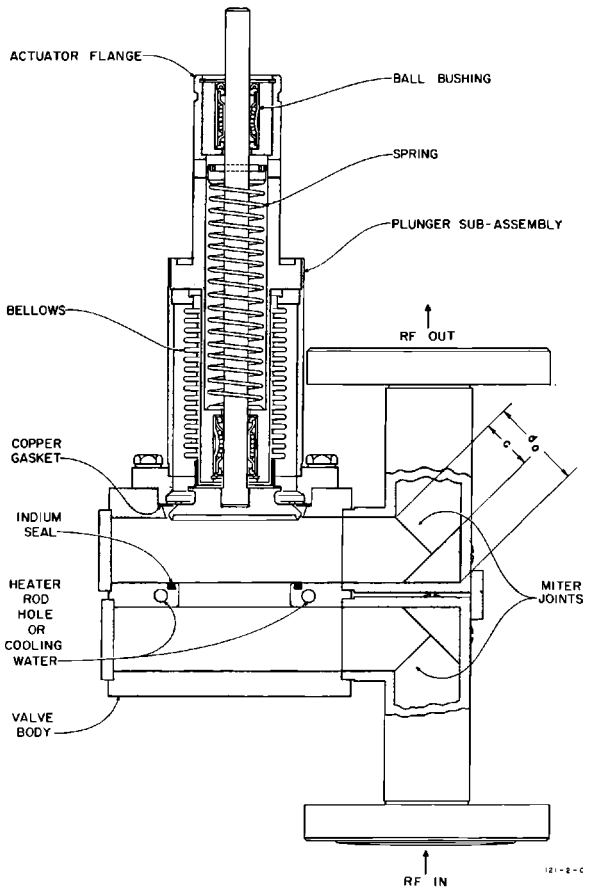

Figure 11-14 Cross-sectional view of waveguide valve assembly.

test units. When the indium seal has become heavily indented after many closures, the surface can be readily renewed by remelting the metal (melting point, 156.6°C) so that it re-forms smoothly in the groove. To achieve this, heater rods are installed in the valve body. The remelting process requires approximately 1½ hours (including cool-down) and can be performed while the valve is installed and operating at low pressures in the accelerator vacuum system.

Considerable attention was given to the problem of casting good indium seals, i.e., achieving an indium-to-stainless steel interface which is free of leak paths and stable under repeated closures. The process which was developed is composed of two steps: a casting or wetting of the indium into the stainless steel groove in a dry hydrogen atmosphere and a remelting of the indium while it is under vacuum. The first step is performed at temperatures

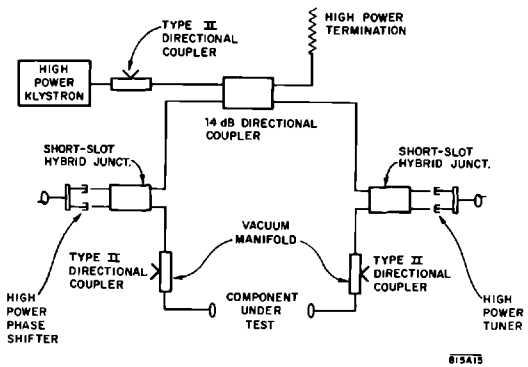

Figure 11-15 Schematic representation of resonant-ring test facility for waveguide vacuum valves.

between 750° and 850°C. The dry hydrogen atmosphere reduces the oxides both on the indium and the stainless steel so that a wetting or interface alloying of the metals can take place. Two runs are made, the first using only a small amount of indium to wet the surfaces of the groove, and the second with the groove filled to the desired level. This entire process is visually monitored since the length of time required and the temperature are not easily specified. They are affected by the dew point of the hydrogen as well as by the initial conditions of the stainless steel, the indium, and even the furnace.

Upon completion of the furnace processing, the assembly is placed on a vacuum station evacuated by an ion-getter pump where the newly cast indium is remelted using external heaters. Vacuum levels on the order of 10^{-5} torr are maintained, but bursts of gas are detectable as the indium melts. The release of these entrapped gases is sometimes accompanied by sputtering of indium onto the surrounding surfaces. The sputtered indium is prevented from reaching the copper-plated inner surfaces of the valve (where it would cause etching) by covering the seal with a hood during this first vacuum remelt. Subsequent remelting of the seal while the valve is installed does not result in significant sputtering.

Each vacuum valve was tested at RF powers of 60-MW peak and 24-kW average power using the resonant ring illustrated in Fig. 11-15. In addition, each valve is cycle-tested 5 times with a maximum allowable leak rate of 1×10^{-8} std cm^3 He/sec.

Directional couplers

A directional coupler is a four-port junction (Fig. 11-16). Providing all ports of this junction are matched, the coupling between ports 1 and 3 and between ports 2 and 4 is zero. Montgomery, Dicke, and Purcell[12] prove that any matched four-port junction is a directional coupler.

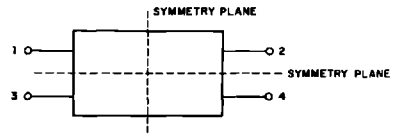

Figure 11-16 Directional coupler schematic.

Three types of directional couplers were used in the waveguide layout. These couplers are listed in Table 11-4 by type, coupling ratio, isolation, and application in the waveguide system. In each case the designs were guided by the necessity to achieve good vacuum performance, compact structure, high isolation, electrical characteristics that are stable with time, and uniformity of coupling ratio.

The properties of the couplers used in the waveguide layout are expressed succinctly by means of the scattering matrix notation. Let $[b_i]$ be a column vector representing the scattered voltages from the four ports, $[a_j]$ be a column vector representing the input voltages, and $[S_{ij}]$ be a 4×4 scattering matrix of the junction. Then

$$[b_i] = [S_{ij}][a_j] \tag{11-9}$$

When $i \neq j$, S_{ij} is the transmission coefficient between ports i and j, and when $i = j$, S_{ii} is the reflection coefficient of port i. Each of the coupler types are reciprocal and symmetrical. Therefore:

$$\begin{aligned} S_{ij} &= S_{ji} \\ S_{11} = S_{22} &= S_{33} = S_{44} \\ S_{12} = S_{21} &= S_{34} = S_{43} \\ S_{13} = S_{31} &= S_{24} = S_{42} \\ S_{14} = S_{41} &= S_{23} = S_{32} \end{aligned} \tag{11-10}$$

Table 11-4 Types and applications of directional couplers in the waveguide layout

Type	*Directional coupler type*	*Nominal coupling ratio (dB)*	*Typical isolation (dB)*	*Waveguide layout application*
I	Short-slot hybrid junction	−3	40	Power divider
II	Modified Bethe hole	−52	80	Sample forward and reflected power at klystron output to monitor klystron performance and provide protection against waveguide arcing
III	Cross guide	−20	40	Sample beam-induced power out of 10-ft accelerator section for use as a reference signal in the automatic phasing system

From Eq. (11-10) the scattering matrix is simplified to

$$S = \begin{bmatrix} S_{11} & S_{12} & S_{13} & S_{14} \\ S_{12} & S_{11} & S_{14} & S_{13} \\ S_{13} & S_{14} & S_{11} & S_{12} \\ S_{14} & S_{13} & S_{12} & S_{11} \end{bmatrix} \tag{11-11}$$

In an ideal well-matched coupler $S_{11} = 0$ and $S_{13} = S_{24} = 0$ representing complete isolation. In this case the scattering matrix reduces to

$$S = \begin{bmatrix} 0 & S_{12} & 0 & S_{14} \\ S_{12} & 0 & S_{14} & 0 \\ 0 & S_{14} & 0 & S_{12} \\ S_{14} & 0 & S_{12} & 0 \end{bmatrix} \tag{11-12}$$

The directional couplers are essentially lossless, and, therefore, the scattering matrix is unitary, i.e.,

$$[S_{ij}][S_{ij}^*] = 1 \tag{11-13}$$

Inserting matrix Eq. (11-12) into Eq. (11-13),

$$|S_{12}|^2 + |S_{14}|^2 = 1 \tag{11-14}$$

$$S_{14}S_{12}^* + S_{12}S_{14}^* = 0 \tag{11-15}$$

If one inserts $S_{14} = |S_{14}|e^{j\phi_4}$ and $S_{12} = |S_{12}|e^{j\phi_2}$ into Eq. (11-15), then

$$\cos(\phi_4 - \phi_2) = 0 \tag{11-16}$$

giving a 90° phase shift between the signals in the output of a matched lossless symmetrical coupler with perfect isolation. Levy[13] shows that with slightly imperfect couplers the phase shift deviation from 90° is related to the isolation. For example, the output signals will deviate 0.1° from 90° in a coupler of which the isolation I is 30 dB, where I in decibels is defined as

$$I_{\text{dB}} = 10 \log_{10} \frac{1}{|S_{13}|^2} \tag{11-17}$$

Levy[13] further shows that in an imperfect coupler the magnitude of the reflected signal at an input port is nearly equal to the magnitude of the signal emerging from the decoupled port as follows;

$$|S_{11}| \approx |S_{13}| \tag{11-18}$$

Measurement of the match looking into a port in a directional coupler provides by Eq. (11-18) a very useful check of the isolation.

In two of the couplers used in the waveguide layout, directivity of coupling is an important consideration. Directivity of a coupler in decibels is defined by the equation

$$D_{\text{dB}} = 10 \log_{10} \frac{|S_{14}|^2}{|S_{24}|^2} \tag{11-19}$$

and is a measure of the capability of the coupler at, say port 4, to distinguish

a "forward" unit signal incident at port 1 from a "backward" unit signal incident at port 2. If the coupling of a directional coupler C in dB is

$$C_{dB} = 10 \log_{10} |S_{14}|^2 \tag{11-20}$$

then the coupling, isolation, and directivity of the coupler are related as follows:

$$D_{dB} = C_{dB} + I_{dB} \tag{11-21}$$

With the relationships developed in the above paragraphs, one can now turn to the design of the couplers used in the network.

Power divider

The three power dividers used in each of the waveguide modules have the function of dividing the power output from a klystron into four equal parts. These power dividers are directional couplers with

$$|S_{12}| = |S_{14}| \tag{11-22}$$

Directional couplers in which Eq. (11-22) holds true are called hybrid junctions because they are analogous to the hybrid repeating coils used in telephone technology. Of the various hybrid junctions available, the short-slot, narrow wall, coupled junction[14,15] was considered to be the most satisfactory because it has high-power handling capacity and each of its ports lies in the same plane. For example, tests indicate that a short-slot hybrid can operate without voltage breakdown at more than 70% of the power capacity of the terminal waveguides. The corresponding power levels in top-wall hybrids and magic T's are 40% and 17%, respectively.

The design of short-slot hybrid junctions (Fig. 11-17) is simplified by analysis of the coupling region using a superposition of even and odd modes. The TE_{10} mode is used as the even mode and the TE_{20} mode is used as the odd mode (Fig. 11-18). The width of the hybrid junction in the coupling region must be large enough to propagate the TE_{20} mode but must be small enough to prevent propagation of the TE_{30} mode (a higher-order even mode) at the operating frequency.

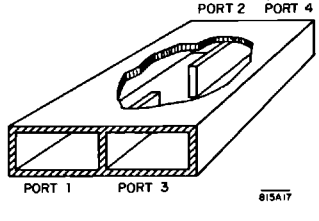

Figure 11-17 Cutaway view of a short-slot hybrid junction showing coupling iris.

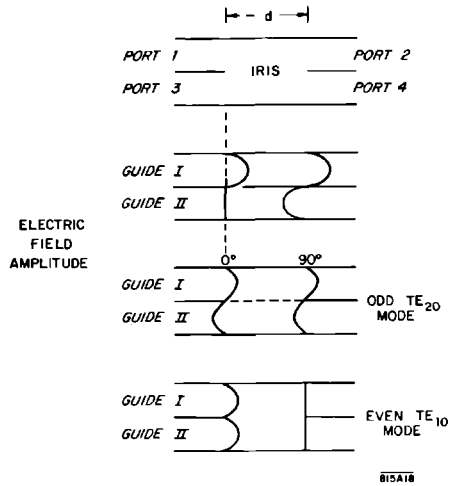

Figure 11-18 Superposition of even and odd modes in a hybrid junction.

The coupling iris is made long enough to provide just 90° phase shift between the even and odd modes as required by Eq. (11-16). Thus, if d is the length of the coupling iris,

$$\frac{2\pi d}{\lambda_{g_e}} - \frac{2\pi d}{\lambda_{g_0}} + \phi_r = \frac{\pi}{2} \tag{11-23}$$

where λ_{g_e} is the guide wavelength in the coupling region of the even TE_{10} mode, and λ_{g_0} is the guide wavelength of the TE_{20} odd mode. The phase shift ϕ_r accounts for reflections at the ends of the coupling iris. At first, ϕ_r is neglected and Eq. (11-23) is solved for d

$$d = \frac{\lambda_0}{4}\left\{\frac{1}{[1-(\lambda_0/\lambda_{c_e})^2]^{1/2} - [1-(\lambda_0/\lambda_{c_0})^2]^{1/2}}\right\} \tag{11-24}$$

where λ_{c_e} and λ_{c_0} are the cut-off wavelengths in the even and odd modes, respectively.

Equation (11-24) is plotted (Fig. 11-19) to provide the initial design length for the coupling iris after a choice is made for the cavity width within the constraints shown for TE_{30} and TE_{20} mode propagation.

An arbitrary choice of cavity width at 5.500 in. permitted operation of the hybrid sufficiently below cutoff for the TE_{30} mode. Hybrid junctions were fabricated with this width and with several different iris lengths near the value 3.850 in. indicated in Fig. 11-19 in order to determine empirically the value ϕ_r and the proper length d to give the desired 90° phase shift.

Fabrication of the hybrid junctions for high-vacuum application required the spacing between the terminal waveguides to be larger than is usual in

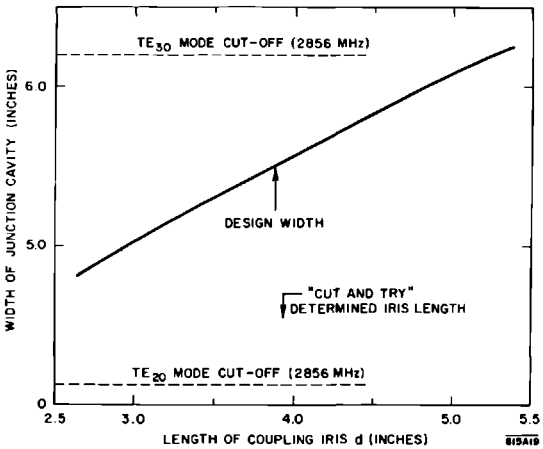

Figure 11-19 Plot of short-slot hybrid junction iris length d as a function of cavity width (assumes $\phi_r = 0$).

nonvacuum junctions. This resulted in a very thick septum at the terminals of the coupling iris. The thick septum gives an appreciable reflection coefficient not only for the even mode but also for the odd mode and this reflection must be cancelled. Stoesser[16] indicates that a septum whose width is 5% of the terminal waveguide width may be corrected by increasing the iris length by 10% above that predicted by Eq. (11-24). It was necessary to use a septum of which the width (0.400 in.) is 14% of the terminal guide width (Fig. 11-20), and compensation for this width was accomplished not only by lengthening the iris to 3.930 in. but also by using capacitive loading at the center of the coupling iris. The centrally located capacitive buttons more strongly affect the even mode guide wavelength than they do the wavelength of the odd mode.

Figure 11-20 Cross-sectional view of hybrid junction showing critical dimensions.

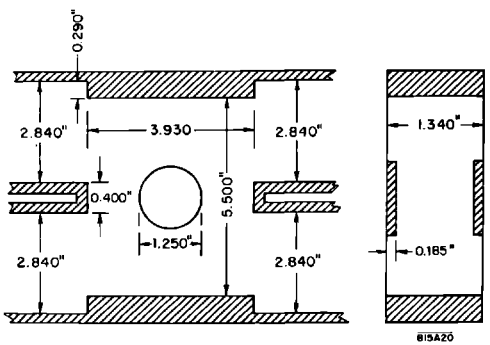

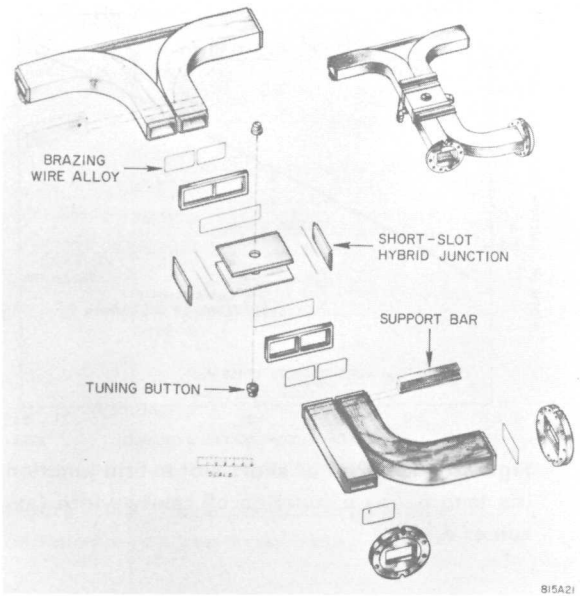

Figure 11-21 "Exploded" view of Type I, 3-dB, directional coupler.

Figure 11-22 Photograph of Type I directional coupler mounted in place in the klystron gallery.

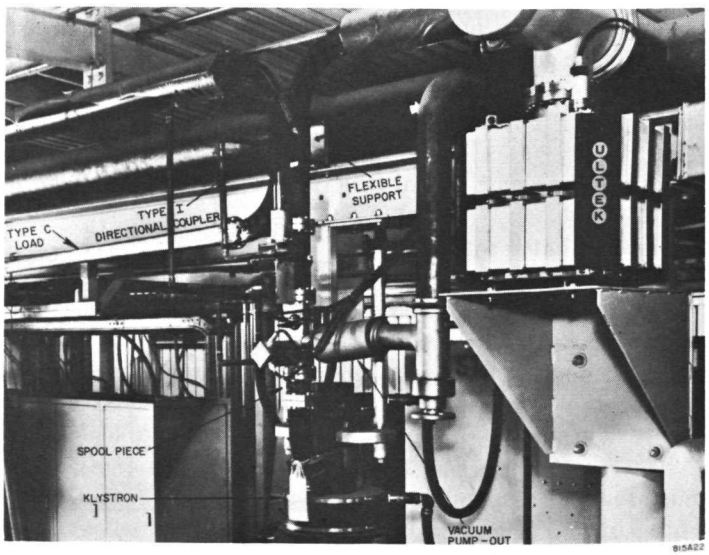

On the other hand, small changes in width of the iris region strongly affects the guide wavelength of the odd mode. It was found by experiment that buttons 1.250 in. in diameter and 0.185 in. high on both bottom and top walls of the junction gave satisfactory performance.

The copper parts for the junctions were designed to be brazed together in a self-jigging method to give near uniform electrical characteristics with little required tuning. Figure 11-21 is an "exploded" view of the hybrid junction. Figure 11-22 is a photograph of a typical power divider with its terminal waveguides and water-cooling connections.

Approximately 800 hybrid junctions were fabricated. The junctions were measured and, after slight tuning by wall deformation, each junction gave a maximum deviation from equal power division of 0.1 dB and isolation values no less than 40 dB (typically 40–50 dB). These values of isolation correspond to input reflection coefficients ($|S_{11}|$, $|S_{22}|$, $|S_{33}|$, and $|S_{44}|$) of less than 0.01.

Modified Bethe hole coupler

A modified Bethe[17] hole coupler was used at the output of the klystron for power sampling. The coupling ratio is -52 dB with 80 dB isolation. In addition to the power sampling function, the Bethe hole coupler unit contains the pump-out for the vacuum connection, the vacuum gauge, and the only fixed tie point of the waveguide system. Figure 11-23 is a photograph of the complete unit.

The modified Bethe hole coupler, which henceforth will be referred to as the "Type II directional coupler," differs from a conventional Bethe hole

Figure 11-23 Photograph of Type II directional coupler.

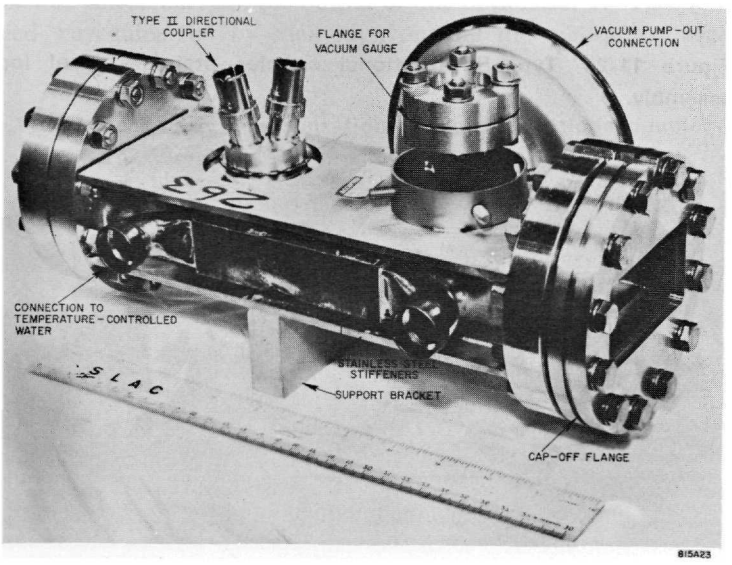

coupler in that the secondary waveguide has been replaced by a coaxial strip line loop which is external to the primary waveguide. The motivations leading to the development of this new type coupler stemmed from the necessity for conserving space and reducing costs. The design used allowed the inclusion of a waveguide pump-out and vacuum gauge in the same space that would have been occupied by a conventional-type coupler. It was possible to design the coupler so that the coaxial strip line loop operated in air while the coupling hole and primary waveguide were a part of the evacuated system. This was made possible by using a dielectric window, as shown in Fig. 11-24. The coupling loop was designed to be a strip line terminated by 50-ohm coaxial cables. The dimensions of the strip line and spacing between the line and ground plane were determined empirically. The dimensions chosen minimized the reflection coefficients $|S_{33}|$ and $|S_{44}|$. The coupling loop was mounted on the primary waveguide in such a way that it could be installed by welding two stainless steel eyelets together. Once a coupling loop assembly (Fig. 11-24) had been fabricated and was found to have a reflection coefficient less than $|0.02|$, the loop was mounted on the waveguide and rotated for optimum directivity which was at least 25 dB and typically 28 dB. The loop assembly was then clamped in the proper orientation and tack-welded. The directivity was then remeasured and if found unchanged the coupling loop assembly was completely heliarc-welded, and the coupler was then ready for final calibration.

The Type II couplers were calibrated using three independent approaches; the intermediate frequency (IF) substitution method (see Fig. 11-25), the calorimetric method at high power, and the RF substitution method after installation in the waveguide network. The coupling values of 250 couplers, as determined by the three techniques, were all identical within a spread of 0.3 dB. Two of the Type II couplers were used as monitors in the resonant

Figure 11-24 Type II directional coupler—stainless steel loop assembly.

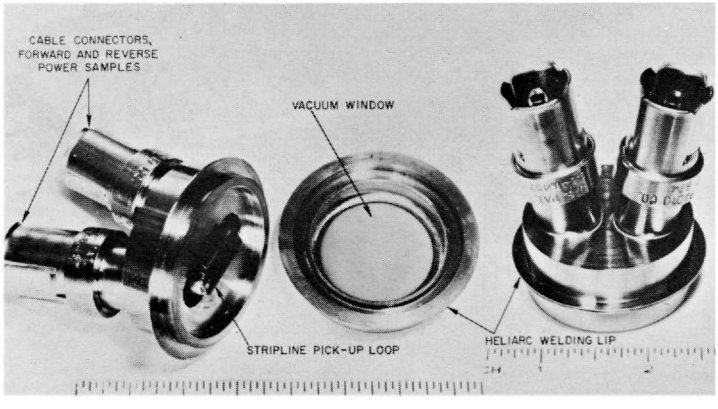

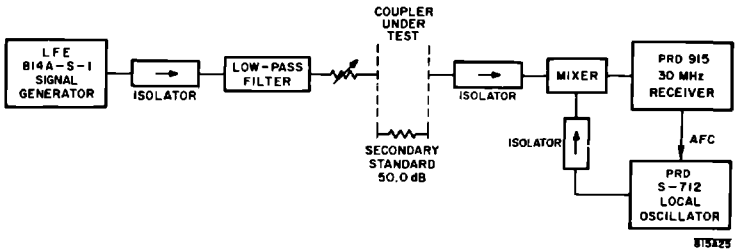

Figure 11-25 Intermediate frequency substitution technique for calibration of Type II directional couplers.

ring to measure ring power. These two couplers operated satisfactorily in the ring at power levels of 90 MW peak and 40 kW average.

The coaxial cables terminating the Type II couplers were 20 ft long, with an approximate attenuation of 3 dB per cable. The coaxial cables from a given coupler were terminated by low-pass filters and strip-line directional couplers (Fig. 11-26) to distribute samples of the forward and reflected power with minimum interaction to a waveguide breakdown detector, and to ports which may be used for monitoring power and pulse shape. The 20-ft cables and the strip-line power distribution package provide the necessary low VSWR termination for the Type II couplers.

Cross guide coupler

In order to provide beam-induced RF signals to operate the automatic phasing system which phases the input to each klystron, a Moreno-type,[18] cross guide coupler was placed between the output of one of the four 10-ft sections of disk-loaded waveguide fed by each klystron and the high-power load

Figure 11-26 Schematic representation of Type II directional coupler—signal sampling network.

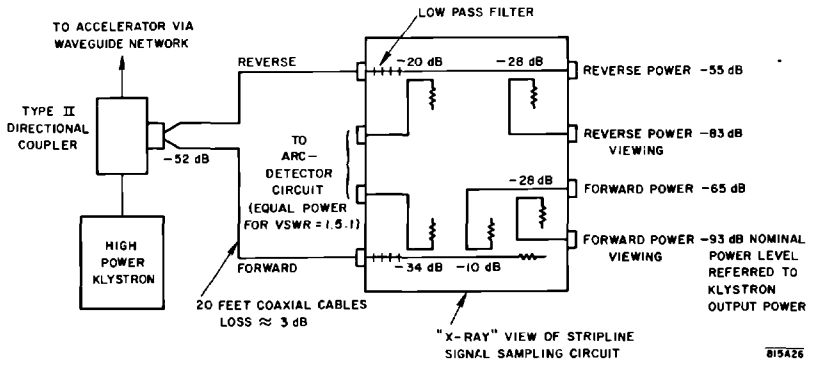

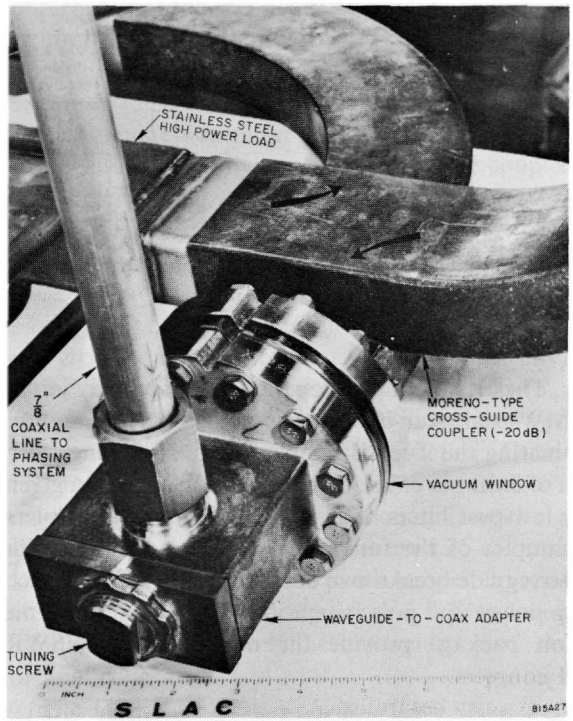

Figure 11-27 Type III directional coupler.

terminating that section. The section used is alternately the second (in an "ABAB" module) and the third (in a "BABA" module). The coupler has a −20 dB coupling coefficient and a directivity of 20 dB. This same coupler design is also used for two applications in the positron source area. The Moreno coupler operates in vacuum, the decoupled port being terminated in an all-metal high vacuum load. The coupled port is connected to a vacuum window (Fig. 11-27) and then to a waveguide-to-coaxial line transition. The coaxial line is a standard $\frac{7}{8}$-in. 50-ohm impedance cable. The assembly of the coupler window and waveguide-to-coaxial line junction was tested to 100-kW peak power without evidence of failure. The 100-kW peak is in excess of the maximum power expected at the coupler when all the power from a klystron drives a single accelerator section.

Waveguide flanges

To facilitate installation, maintenance, and repair of the rectangular waveguide network, it was necessary to develop a rectangular waveguide flange joint which would make a high vacuum seal and handle high RF powers.

The specifications established for the flanges were as follows:

1. No organic seals or gaskets were to be used in the flange joints.
2. The flange pair when assembled with a gasket should provide a joint which has a VSWR of 1.015 or less at a frequency of 2856 $\pm$ 100 MHz.
3. The flange pair should be capable of transmitting 40-kW average and 90-MW peak power.
4. The flange pair should withstand at least twenty opening and closing cycles, provided a new gasket was used each time the seal was remade.
5. The completed seal should have a leak rate not greater than 2×10^{-10} std cm^3 He/sec.
6. The assembled flange pair should be leak tight when subjected to a bake-out cycle consisting of heating at a rate of 100°C/hour to a peak of 560°C, holding at this temperature for 48 hours and cooling at a rate of 100°C/hour.
7. The maximum angular mismatch between two assembled flanges should not exceed 0.25°.
8. The maximum offset between two assembled flanges should not exceed 0.010 in. in any symmetry plane.

The specification regarding leak rate during a bake-out cycle resulted from klystron manufacturing experience. Paradoxically, the final flange used in the rectangular waveguide network is not yet in use on the klystrons because klystron manufacture was started prior to the development of the rectangular waveguide network, and a different flange design is used. In order to transform to the klystron flange, a spool piece is inserted between the terminal point of the rectangular waveguide and the klystron. The spool piece comprises a short piece of waveguide with the specially developed Skarpaas[19] flange on one end and a Merdinian[20] flange matching the klystron on the other end. An additional reason for use of the spool piece is to protect the flange on the end of the major waveguide system. When a klystron is being replaced, only the spool piece flange is subject to risk of accidental damage. If this occurs, it can easily be replaced.

It is easier to make a reliable vacuum joint with a circular seal. However, microwave continuity requires a high current joint which follows the rectangular periphery of the waveguide, at least across the broad walls. The RF currents for the dominant TE_{10} mode flow longitudinally on the broad walls and only in the transverse direction on the narrow walls. Hence good contact is not necessary on the narrow walls of the waveguide at the joint. Good contact along the broad walls of the waveguide is achieved by making the male flange slightly conical and the female flange flat. The vacuum requirement is met by a circular male–female configuration on the mating flanges which shears into the copper gasket. In assembly, the first points of contact with the gasket are in the center of each of the strips forming the rectangular aperture in the gasket. As the bolts are tightened, a near line contact is obtained along each strip. It can be seen from Fig. 11-28 that the only regions of

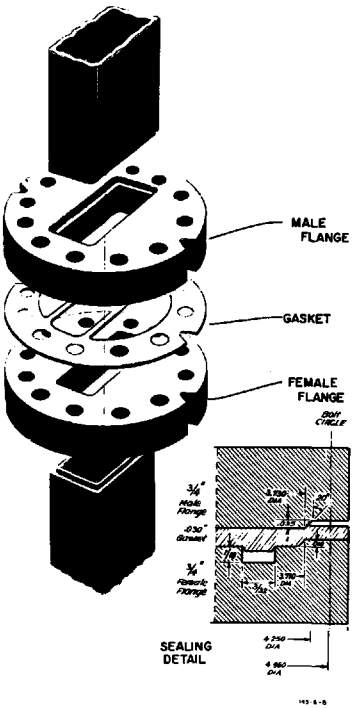

Figure 11-28 Waveguide flange (Skarpaas) vacuum seal and copper gasket.

high-pressure contact between the flanges and the gasket are these two narrow strips of copper coplanar with each broad wall of the waveguide and an outer copper ring which forms the vacuum joint. The width of the copper strips was kept small to insure high contact pressure and to minimize the vacuum virtual leak problem. The void between the flanges that is formed between the strips and the circular vacuum seal is evacuated by means of a pump-out groove which opens into the narrow wall of the waveguide.

The critical alignment of the flanges during assembly is achieved by a clamp band which holds two precision dowels in the precision alignment "V" slots during the operation of inserting and torquing the bolts. Approximately 6000 pairs of flanges were fabricated and installed in the waveguide network with no difficulties during installation or failures to date, which is 2 yr after installation.

Waveguide loads

High-power and low-power vacuum RF loads were required to terminate each 10-ft section of the disk-loaded accelerator waveguide and to terminate the power dividers. A number of design approaches were considered, some

of which used lossy dielectrics. An all-metal design was finally adopted, using a resistive coating on the inside walls of tapered rectangular waveguide to dissipate the RF power in the form of skin losses. The basic construction used was the same for both the low-power and the high-power loads. The high-power loads were water cooled by means of copper tubes brazed onto the outside walls.

The heat exchange problem for the high-power load was simplified by making the rate of heat dissipation along the length of the load as uniform as practical.

The power, $P(z)$, in the load should decrease linearly from the input power P_0 at $z = 0$ to zero at $z = L$, where L is the length of the load. Thus,

$$P(z) = P_0\left(1 - \frac{z}{L}\right) \tag{11-25}$$

Differentiating Eq. (11-25) gives

$$\frac{dP(z)}{dz} = -\frac{P_0}{L} \tag{11-26}$$

The attenuation constant, $\alpha(z)$, is defined as follows:

$$\alpha(z) = -\frac{1}{2P(z)}\frac{dP(z)}{dz} \tag{11-27}$$

Combining Eqs. (11-26) and (11-27) gives

$$2\alpha(z)P(z) = \frac{P_0}{L} \tag{11-28}$$

Substituting Eq. (11-25) into Eq. (11-28) gives

$$\alpha(z) = \frac{1}{2(L - z)} \text{ Np/unit length} \tag{11-29}$$

The attenuation constant α for the TE_{10} mode in rectangular waveguide is given by the following relationship:

$$\alpha = \frac{2R_s v^2}{a\eta[1 - v^2]^{1/2}} + \frac{R_s}{b\eta[1 - v^2]^{1/2}} \tag{11-30}$$

where

R_s is the surface resistivity of the waveguide walls
a and b are the waveguide cross section dimensions (Fig. 11-5)
η is the intrinsic impedance of the medium
v is λ/λ_c, the ratio of the free space wavelength to the cutoff wavelength in the waveguide

Equation (11-30) illustrates that $\alpha(z)$ may be controlled by varying dimensions a and b of the cross section if the surface resistivity is held constant. Large values of α can be obtained by reducing the cross section as a function of length.

Ideally, a load should absorb all incident waves with no reflection, which requires $\alpha(z)$ to be infinite when $z = L$. However, in a practical load a one-way attenuation of 15 dB produces a reflection coefficient $|S_{11}|$ of 0.03. A tapered load, 5 ft in length, that is properly coated can be readily made to give 15 dB attenuation.

Surface resistivity is defined as

$$R_s = \frac{1}{\sigma\delta} = \left(\frac{\pi f \mu}{\sigma}\right)^{1/2} \text{ohms/square} \tag{11-31}$$

where

σ = conductivity in mhos/meter
δ = skin depth, in meters
f = frequency in hertz
μ = permeability in henrys/meter

Equation (11-31) indicates that for good attenuation, an absorbing material should have low electric conductivity and high permeability at a given frequency. In addition, the absorbing material must be stable and have good vacuum properties for evacuated waveguide networks. Kanthal,* an iron alloy (iron, 20–30% chromium, 5% aluminum, and traces of manganese), meets these requirements reasonably well. There is also considerable vacuum experience with the material as an absorber in high-power microwave tubes. Accordingly, Kanthal was selected as the absorber material. Nalos[21] measured the resistivity of Kanthal to be 1.2 ohms/square for a film 0.002 in. thick on a copper base using a resonant cavity technique. Experiments with films 0.006–0.010 in. thick on a stainless steel base with WR-284 waveguide configuration indicated that 0.7 dB/ft attenuation could be achieved at 2856 MHz. This attenuation corresponds to a surface resistivity of 1.86 ohms/square. In both cases, Kanthal wire was flame-sprayed onto the base material. The higher resistivity apparently resulted from the greater thickness of the film and from increased surface roughness that accompanied the thick film. Films thicker than 0.008 in. did not result in increased attenuation. Conductivity of Kanthal was measured to be 7.32×10^3 mhos/meter ($\pm 10\%$). From Eq. (11-31) the skin depth of Kanthal at 2856 MHz is approximately 0.003 in.

To achieve the most economical load design, a straight taper in both the a and b dimensions from the WR-284 waveguide size was used down to a cross section $a' = 2.08$ in. (just above cutoff at 2856 MHz) and $b' = 0.280$ in. The stainless steel walls used to fabricate the taper were prepared for welding

* Registered by the Kanthal Corporation, 1 Wooster, Bethel, Connecticut; special electric resistance alloys.

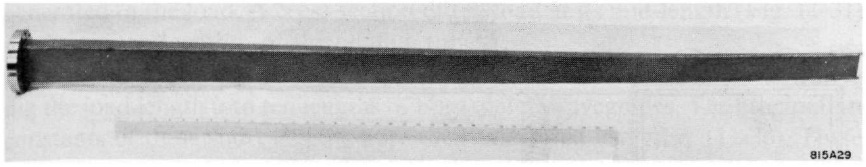

Figure 11-29 Photograph of stainless steel low-power vacuum load.

by cleaning for vacuum, then by sandblasting (to increase the surface roughness for good bonding to the Kanthal film), and then by flame-spraying Kanthal wire to a uniform depth inside a mask that protected the edge to be welded. The walls were then tack-welded together to form a taper, using an aluminum mandrel. The final welding took place in an automatic heliarc welder to insure a full penetration weld along the corners.

After welding, the loads were vacuum baked at 600°C for 24 hours with the terminal vacuum level at 10^{-6} torr. Approximately 2000 loads, half high-power and the other half low-power, were fabricated. The loads typically had an input reflection coefficient $|S_{11}| = 0.05$ before tuning. The low-power loads (Fig. 11-29) were tuned to give $|S_{11}| < 0.02$ by dimpling the stainless steel walls. The high-power loads (Fig. 11-30) were tuned under high-power operation on a test stand. Processing the load at high power is a procedure in which the input power is increased slowly in steps to outgas the load with RF. Foreign materials with low work functions cause multipactoring and require

Figure 11-30 Photograph of stainless steel high-power vacuum load.

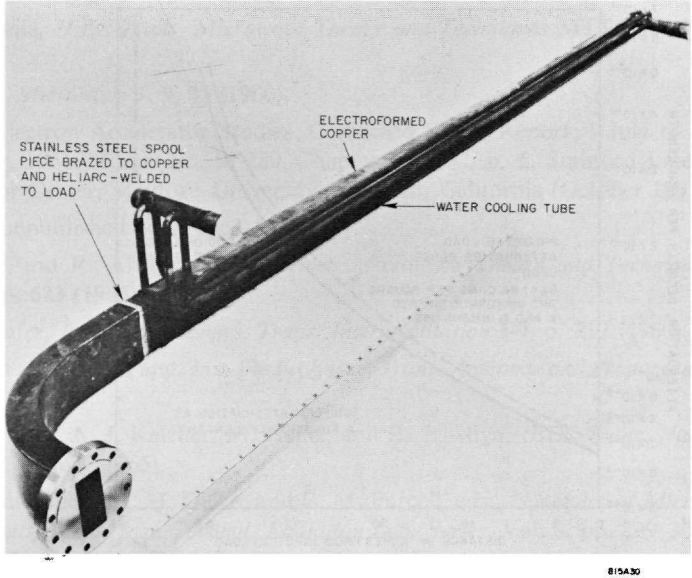

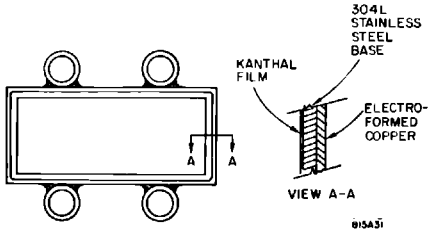

Figure 11-31 Cross-sectional view of high-power RF load.

sufficient local heating to burn them off. After processing, the high-power loads were tuned to minimize the reflection coefficient. Some of the high-power loads were tested at power levels of 18 MW peak with reflection coefficients less than 0.17. Most of the high-power loads were tested only to power levels of 8 to 10 MW peak power. The maximum input power to the loads is approximately 2 MW peak, when one klystron is used to drive four 10-ft sections of disk-loaded waveguide.

Attachment of cooling tubes to the high-power loads was accomplished by first electroforming a thick layer of copper onto the outside walls of the load and then brazing the copper tubes to the surface. The electroformed copper provides a good thermal conduction path to the water-cooling tubes for heat

Figure 11-32 Comparison of predicted load attenuation with uniform attenuation per unit length of load.

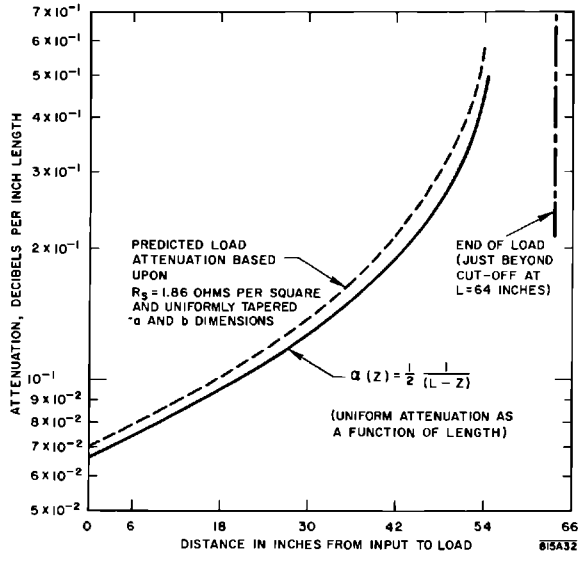

generated in the load. A cross section of the load at its mid-length (Fig. 11-31) illustrates the location of the cooling tubes.

The predicted rate of heat dissipation of the load was determined by dividing the load length into ten lengths of nontapered waveguides. The attenuation constants of these short lengths were then calculated using Eq. (11-30). These constants were compared to the desired values from Eq. (11-29). (See Fig. 11-32). No hot spots in the loads were observed, and the minimum one-way attenuation of 15 dB was achieved. During 2 yr of operation only one load failed due to multipactoring problems.

Acknowledgments

The authors would like to acknowledge the creative contributions of the following people whose efforts were instrumental in the successful completion of the rectangular waveguide network: M. Adams, R. Alvarez, C. Angelos, R. Borghi, R. Chapton, M. Gan, A. Guidi, A. Keicher, R. Lam, A. Lisin, E. Marshall, R. Messimer, J. Pope, C. Rasmussen, K. Skarpaas, H. Soderstrom, B. Stillman, J. Weaver, and H. Zaiss.

References

1 G. L. Matthaei, L. Young, and E. M. T. Jones, *Microwave Filters, Impedance-Matching Networks, and Coupling Structures*, McGraw-Hill, New York, 1964, p. 910.

2 H. J. Riblet, *Proc. Inst. Radio Engrs.* **40**, 180–184 (1952).

3 D. Tsang and A. Keicher, unpublished notes.

4 L. G. Virgile, *IEEE Trans. Microwave Theory and Techniques* **MTT-5**, p. 247 (1957).

5 L. Young, *Microwave J.* **9**, 45 (1966).

6 "Linear Electron Accelerator Studies; Combined Status Report; 1 July to 30 September, 1961," Rept. No. M-280, Chapter III, F-2, p. 5, Stanford Linear Accelerator Center, Stanford University, Stanford, California (October 1961).

7 A. Lisin, unpublished note (1963).

8 J. Weaver and R. Alvarez, *IEEE Trans. Microwave Theory and Techniques* **MTT-14**, p. 623 (1966).

9 G. E. Schafer, *Inst. Radio Engrs. Trans. Instrumentation* **I-9**, p. 217 (1960).

10 G. Swarup and K. S. Yang, *Inst. Radio Engrs. Trans. Antennas and Propagation* **AP-9**, p. 75 (1961).

11 A. L. Eldredge, A. J. Keicher, M. Heinz, and R. J. Allyn, *IEEE Trans. Nucl. Sci.* **NS-12**, p. 694 (1965).

12 C. G. Montgomery, R. H. Dicke, and E. M. Purcell, eds., *Principles of Microwave Circuits, Mass. Inst. Technol. Radiation Lab. Series*, Vol. 8, pp. 299–301, McGraw-Hill, New York, 1948.

13 R. Levy, "Directional Couplers," in *Advan. Microwaves* (L. Young, ed.), Vol. 1, p. 124, Academic Press, New York, 1966.

14 M. Surdin, *J. Inst. Elec. Engrs.* (*London*) (Pt. IIIA) **93**, 725 (1946).

15 H. J. Riblet, "Waveguide hybrid," U.S. Patent No. 2,739,288 (filed March 17, 1950).

16 W. Stoesser, *Frequenz* (*Berlin*) **14** (4), 117 (April 1960).

17 H. A. Bethe, "Theory of Side Windows in Waveguides," MIT Radiation Lab. Rept. No. 43-27, Massachusetts Institute of Technology, Cambridge, Massachusetts (1943); also, H. A. Bethe, "Theory of Diffraction by Small Holes," *Phys. Rev.* **66**, 163 (1944); also, R. L. Kyhl, "Directional Couplers," in *Techniques of Microwave Measurements, Mass. Inst. Technol. Radiation Lab. Series* (C. G. Montgomery, ed.), Vol. 11, p. 858, McGraw-Hill, New York, 1947.

18 T. Moreno, "A New Directional Coupler for Waveguides," unpublished report, Sperry Gyroscope Co., Inc., Garden City, New York, July 17, 1946.

19 K. Skarpaas, "Microwave waveguide coupling seal," U.S. Patent No. 3,212,035, (filed December 20, 1963).

20 G. Merdinian, unpublished notes.

21 E. J. Nalos, "Loss for High Power TWT's," unpublished note, General Electric Microwave Laboratory, Palo Alto, California, March 1955.